

Hidden half-metallicity

San-Dong Guo^{*}

School of Electronic Engineering, Xi'an University of Posts and Telecommunications, Xi'an 710121, China

Pan Zhou[†]

*Key Laboratory of Low Dimensional Materials and Application Technology of Ministry of Education,
School of Materials Science and Engineering, Xiangtan University, Xiangtan 411105, China*

Half-metals, featuring ideal 100% spin polarization, are widely regarded as key materials for spintronic and quantum technologies; however, the half-metallic state is intrinsically fragile, as it relies on a delicate balance of exchange splitting and band filling and is therefore highly susceptible to disorder, external perturbations, and thermal effects. Here we introduce the concept of hidden half-metallicity, whereby the global electronic structure of a symmetry-enforced net-zero-magnetization magnet is non-half-metallic, while each of its two symmetry-related sectors is individually half-metallic, enabling robust 100% spin polarization through a layer degree of freedom. Crucially, the vanishing net magnetization of the entire system suppresses stray fields and magnetic instabilities, rendering the half-metallic functionality inherently more robust than in conventional ferromagnetic half-metals. Using first-principles calculations, we demonstrate this mechanism in a *PT*-symmetric bilayer CrS₂, and further show that an external electric field drives the system into a seemingly forbidden fully compensated ferrimagnetic metal in which hidden half-metallicity persists. Finally, we briefly confirm the realization of hidden half-metallicity in altermagnets, establishing a general paradigm for stabilizing half-metallic behavior by embedding it in symmetry-protected hidden sectors and opening a new route toward the design and discovery of unprecedented half-metallic phases.

Introduction.— Half-metals, in which one spin channel is metallic while the other is insulating, exhibit ideal 100% spin polarization and are therefore regarded as key materials for high-performance spintronic devices [1]. Such perfect spin selectivity can give rise to ultrahigh tunneling magnetoresistance (TMR) and enable substantial improvements in magnetic storage density and energy efficiency [2]. Despite these appealing properties, the half-metallic state is intrinsically fragile, as it relies on a delicate balance of exchange splitting and band filling and is thus highly susceptible to disorder, structural imperfections, external perturbations, and thermal fluctuations. As a result, many materials predicted to be half-metallic under ideal conditions fail to retain full spin polarization in realistic experimental environments. Collinear magnets can be broadly classified into net-zero-magnetization and nonzero-magnetization systems [3–6]. While half-metallicity can be realized in ferromagnets, ferrimagnets, and fully-compensated ferrimagnets—among which the latter are particularly attractive due to their vanishing net magnetic moment and reduced stray fields [5, 7–9], the symmetry-enforced degeneracy between spin-up and spin-down electronic states rigorously forbids conventional half-metallicity in *PT*-antiferromagnets (*PT*) of space inversion symmetry (*P*) and time-reversal symmetry (*T*) and altermagnets.

The concept of hidden physics offers a promising strategy to overcome such symmetry-imposed constraints. A paradigmatic example is hidden spin polarization in globally centrosymmetric systems composed of locally non-centrosymmetric sectors, where spin-split electronic states exist in real space but cancel in the bulk [10–14].

This insight has stimulated extensive exploration of a broad class of hidden phenomena [14], including hidden orbital polarization, hidden Berry curvature, and hidden valley polarization [15–17]. More recently, this framework has been extended to magnetic systems [18], leading to the proposal of hidden altermagnetism, in which a globally *PT*-symmetric phase exhibits zero net spin polarization while each symmetry-related sector hosts finite local spin splitting [19, 20]. Very recently, hidden altermagnetism has been experimentally confirmed in Cs_{1- δ} V₂Te₂O using neutron diffraction and spin-resolved angle-resolved photoemission spectroscopy [21]. In parallel, the concept of hidden fully-compensated ferrimagnetism has also been introduced, further enriching the landscape of hidden magnetic states [22].

Motivated by these developments, we explore whether half-metallicity can be realized in a hidden manner in net-zero-magnetization magnets that are globally forbidden by symmetry from hosting conventional half-metallic states. In this work, we propose the concept of hidden half-metallicity, in which two symmetry-related sectors are each individually half-metallic, while their contributions cancel in the global electronic structure, resulting in zero net spin polarization. This unique combination of local 100% spin polarization and vanishing total magnetization offers an intrinsically more stable alternative to conventional ferromagnetic half-metals. Using first-principles calculations, we demonstrate the feasibility of this concept in a *PT*-symmetric bilayer CrS₂ as a prototypical example.

Fundamental mechanism.— For a collinear

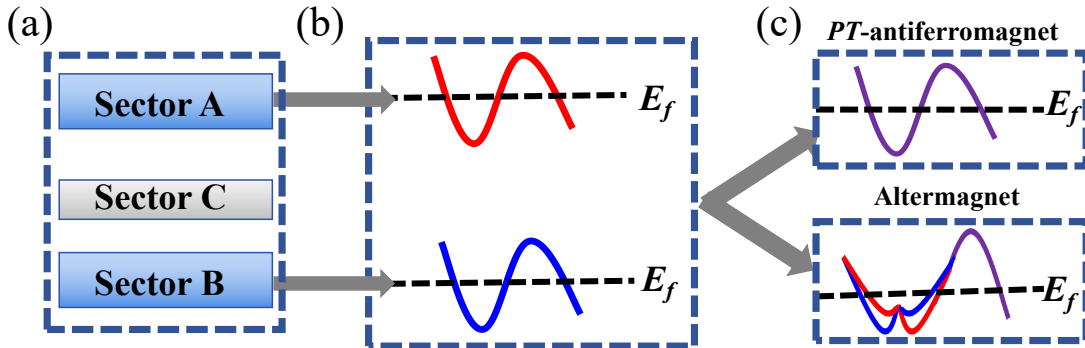


FIG. 1. (Color online)(a):this system belongs to the class of symmetry-enforced net-zero-magnetization magnets, encompassing primarily *PT*-antiferromagnets and altermagnets. The system is composed of three sectors: A, B, and C. The electronic states near the Fermi level are primarily contributed by A and B, while those from C lie far from the Fermi energy. (b): the sectors A and B are half-metallic, exhibiting opposite spin polarizations. (c): viewed globally, the energy band is either spin-degenerate or exhibits altermagnetic spin-splitting. In (b, c), the blue, red, and purple curves denote the spin-up, spin-down, and spin-degenerate bands, respectively, while the horizontal black dashed line indicates the Fermi level.

symmetry-enforced net-zero-magnetization magnet (for example, *PT*-antiferromagnets and altermagnets), the spin-up and spin-down bands satisfy the relation:

$$E_{\uparrow}(\vec{k}) = [C_2 \parallel O] E_{\uparrow}(\vec{k}) = E_{\downarrow}(O\vec{k}) \quad (1)$$

where the O denotes P or rotational (C) or mirror (M) symmetry, and the C_2 is the two-fold rotation perpendicular to the spin axis in spin space. According to [Equation 1](#), we obtain:

$$g_{\uparrow}(E) = \sum_{\vec{k}} \delta[E - E_{\uparrow}(\vec{k})] = \sum_{\vec{k}} \delta[E - E_{\downarrow}(O\vec{k})] \quad (2)$$

As \vec{k} runs over the entire first Brillouin zone (BZ), $O\vec{k}$ also spans the entire BZ. Therefore, [Equation 2](#) can be rewritten as:

$$\sum_{\vec{k}} \delta[E - E_{\downarrow}(O\vec{k})] = \sum_{\vec{k}'} \delta[E - E_{\downarrow}(\vec{k}')] = g_{\downarrow}(E) \quad (3)$$

where the $g_{\uparrow}(E)$ and $g_{\downarrow}(E)$ are defined as spin-up and spin-down densities of states (DOS). According to [Equation 2](#) and [Equation 3](#), the $g_{\uparrow}(E)$ and $g_{\downarrow}(E)$ are identical ($g_{\uparrow}(E)=g_{\downarrow}(E)$) in collinear symmetry-enforced net-zero-magnetization magnets. This implies that half-metallic states are absent in collinear symmetry-enforced net-zero-magnetization magnets, because such states require an imbalance between the spin-up and spin-down DOS.

Although a collinear symmetry-enforced net-zero-magnetization magnet cannot be half-metallic as a whole, the local half-metallicity can still emerge once the spatial 'layer' degree of freedom is introduced. In this study, we introduce the concept of hidden half-metallicity (See [Figure 1](#)), which posits that the 'local' half-metallicity with only one spin channel crossing the Fermi level can arise, when the specific atomic layer marked with sector A or B is ferromagnetic (FM), ferrimagnetic or

fully-compensated ferrimagnetic half-metal. In other words, the magnetic atoms in sectors A and B can be coupled either ferromagnetically or antiferromagnetically (ferrimagnetic or fully-compensated ferrimagnetic half-metal). When the magnetic atoms of sectors A and B are connected by $[C_2 \parallel P]$ symmetry, their local spin polarizations are opposite, leading to spin degeneracy. In a two-dimensional (2D) system, the $[C_2 \parallel M_z]$ symmetry can also enforce spin degeneracy (For 2D systems, the wave vector k only has in-plane components, and then $E_{\uparrow}(k)=[C_2 \parallel M_z]E_{\uparrow}(k)=E_{\downarrow}(k)$). If the magnetic atoms in sectors A and B are linked by a $[C_2 \parallel C/M]$ -symmetric connection, it will give rise to altermagnetic spin-splitting.

Identifying bulk materials that harbor hidden half-metallicity remains a challenge. Here, we realize hidden half-metallicity via an alternate bilayer-stacking-engineering strategy. Employing an analogous construction scheme in ref.[17], we can engineer a bilayer system with $[C_2 \parallel P]$ or $[C_2 \parallel M_z]$ symmetry by using the half-metallic monolayer as the basic building unit. For altermagnetic bilayer systems, some general construction strategies have also already been proposed[23–26]. Here, we elucidate hidden half-metallicity in detail by taking the *PT*-symmetric CrS_2 bilayer with antiferromagnetic (AFM) interlayer coupling as a representative case.

Computational detail.— Density functional theory[27, 28] calculations are performed by using the Vienna ab initio simulation package (VASP)[29–31] within the projector augmented-wave (PAW) method. We use the generalized gradient approximation (GGA) of Perdew, Burke, and Ernzerhof (PBE)[32] as the exchange-correlation functional. A kinetic energy cutoff of 500 eV, total energy convergence criterion of 10^{-8} eV and force convergence criterion of $0.001 \text{ eV} \cdot \text{\AA}^{-1}$ are adopted. We add Hubbard correction with $U=3.00$ eV[33] and 3.68 eV[34] for *d*-orbitals of Cr and V atoms

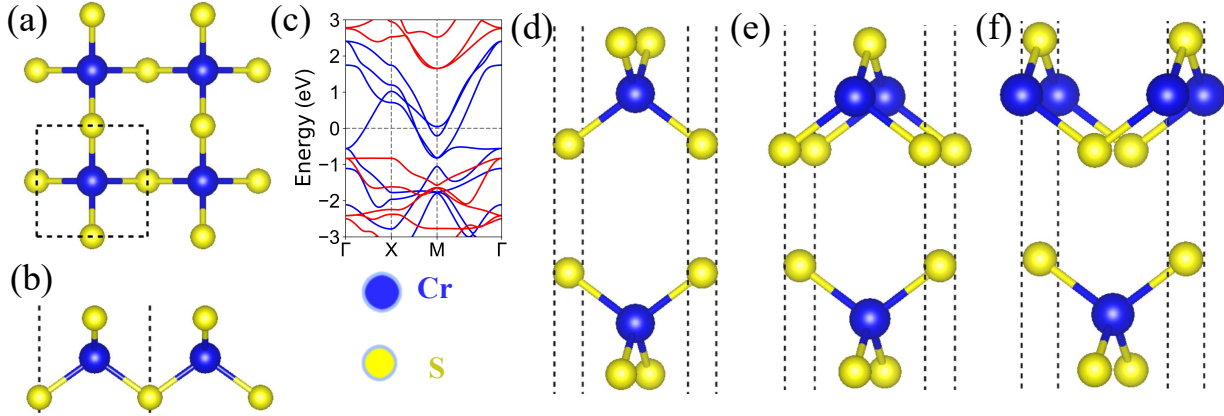


FIG. 2. (Color online) For CrS_2 , (a, b, c): the crystal structures and energy band structures of monolayer; (d, e, f): the AA-, AB-, and AC-stacked bilayer crystal structures. In (c), the spin-up and spin-down channels are depicted in blue and red.

TABLE I. For AA-, AB-, and AC-stacked bilayer CrS_2 , the energies (meV) of AFM and FM interlayer couplings relative to that of AC-stacking with AFM interlayer coupling.

| | AA | AB | AC |
|-----|-------|------|------|
| AFM | 102.8 | 54.4 | 0 |
| FM | 105.6 | 52.2 | -2.1 |

within the rotationally invariant approach proposed by Dudarev et al[35]. The vacuum slab of more than 20 \AA is added to avoid the physical interactions of periodic cells. We use a $15 \times 15 \times 1$ Monkhorst-Pack k -point meshes to sample the BZ for structure relaxation and electronic structure calculations. The dispersion-corrected DFT-D3 method[36] is adopted to describe the van der Waals interactions.

Material realization.— Monolayer CrS_2 has been predicted to be stable in dynamics, thermodynamics, and mechanics[33]. The CrS_2 contains three atomic sublayers with one Cr atom sandwiched between two S atomic layers, as shown in Figure 2 (a, b). Each Cr atom is connected with four S atoms, constituting a distorted tetrahedron. The CrS_2 crystallizes in the $P\bar{4}m2$ space group (No.115), lacking lattice symmetry P . To determine the magnetic ground state, we construct three magnetic configurations, including FM, AFM1 and AFM2 orderings (see FIG.S1[37]). Our calculations demonstrate that the FM configuration is the ground state, exhibiting an energy per unit cell that is 414 meV and 242 meV lower than those of the AFM1 and AFM2 configurations, respectively. The optimized lattice constants are $a=b=3.637 \text{ \AA}$ with FM ordering.

Figure 2 (c) presents the spin-resolved energy band structures of monolayer CrS_2 . The spin-up channel intersects the Fermi level, whereas the spin-down channel exhibits an indirect band gap of 2.48 eV. Consequently, monolayer CrS_2 behaves as a metal for spin-up channel and as a semiconductor for spin-down channel,

manifesting intrinsic half-metallicity. The observed half-metallicity is attributed to Hund's-rule splitting of the partially filled d -orbitals of the Cr atom, accompanied by weak d - p orbital hybridization[38]. Consequently, charge transport is governed exclusively by the spin-up channel, yielding 100% spin polarization.

Next, we build PT -symmetric bilayer CrS_2 using the construction scheme[17]. Initially, we take the CrS_2 as the basic building unit, defined as sector B. Through a mirror operation M_z , the sector A can be derived from the sector B. The resulting bilayer (see Figure 2 (d) as AA-stacking) possesses not only M_z symmetry but also acquires P symmetry automatically, because monolayer CrS_2 intrinsically exhibits C_{2z} symmetry ($P=C_{2z}M_z$). In general, AA-stacking is not the energetically most favorable configuration[19]. Based on AA-stacking, the AB- and AC-stackings (see Figure 2 (e) and (f)) can be constructed by translating the upper sublayer by $\vec{a}/2$ along the a -axes and $(\vec{a}+\vec{b})/2$ along the diagonal direction, respectively. The AA-, AB- and AC-stackings crystallize in the $Pmmm$ (No.47), $Pmma$ (No.51) and $Pmmn$ (No.59), and they all have lattice symmetry P .

For monolayer CrS_2 , the energies of AFM1 and AFM2 orderings are several hundred meV above that of FM ordering, whereas the interlayer magnetic interaction is typically smaller than 10 meV[17, 19, 26]. We therefore fix the intralayer FM ordering and vary only the interlayer magnetic coupling (FM or AFM) to determine the magnetic ground state of the bilayer. The energies of the three stacking arrangements with the two interlayer magnetic couplings are summarized in Table I. It is found that the AC stacking is significantly lower in energy than both AA and AB stackings, and the following discussion focuses exclusively on the AC-stacked bilayer. Unfortunately, the ground state of AC-stacked bilayer exhibits FM interlayer coupling. Nevertheless, a transition between FM and AFM interlayer coupling can be realized by modulating the interlayer spacing d (see

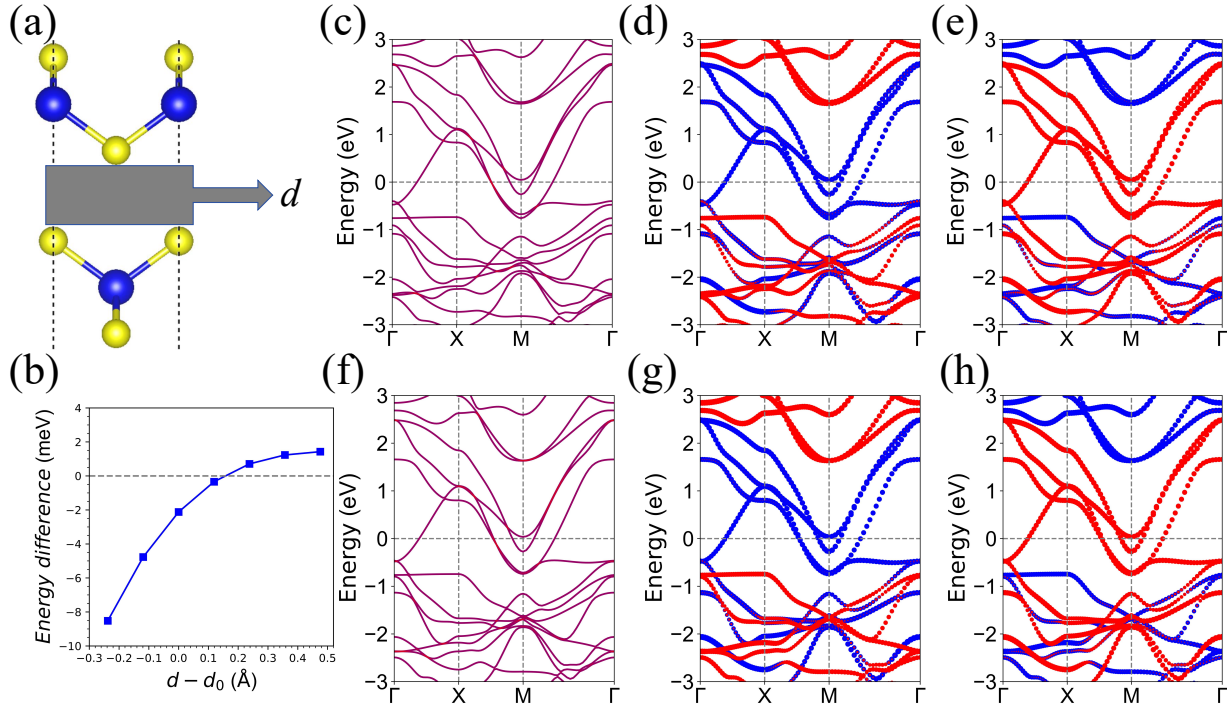


FIG. 3. (Color online) For AC-stacked bilayer CrS_2 , (a): the schematic illustration of tuning the interlayer spacing between the lower and upper layers; (b): the energy difference between FM and AFM interlayer couplings versus $d - d_0$, where the d_0 denotes the equilibrium interlayer distance; (c, d, e): the total energy band structure along with the spin-resolved projections onto the lower and upper layers with the equilibrium interlayer distance; (f, g, h): the total energy band structure along with the spin-resolved projections onto the lower and upper layers with $d - d_0$ being 0.48 Å. In (c, d, e, f, g, h), the blue, red, and purple curves denote the spin-up, spin-down, and spin-degenerate bands, respectively. In (d, e, g, h), the weighting coefficient is proportional to the circle size.

Figure 3 (a)). The interlayer spacing can be tuned with laser shocking (LS) engineering. In $\text{FePSe}_3/\text{Fe}_3\text{GeTe}_2$ heterostructures, the LS can permanently reduce the interlayer spacing from 7.4 Å to 4.6 Å[39]. The energy difference between FM and AFM interlayer couplings as a function of $d - d_0$ is plotted in Figure 3 (b), where the d_0 denotes the equilibrium interlayer distance. It is found that reducing the interlayer separation favors FM coupling, whereas expanding the interlayer distance promotes AFM interlayer coupling. When $d - d_0$ exceeds 0.15 Å, the AC-stacked bilayer switches from FM to AFM interlayer coupling.

For comparison, the band structures of the interlayer AFM-coupled AC bilayer are presented in Figure 3 for both $d - d_0 = 0$ and 0.48 Å, along with the spin-resolved projections onto the lower and upper layer CrS_2 . Owing to PT symmetry, the bands are manifestly spin-degenerate and exhibit no half-metallic character. Nevertheless, when the layer degree of freedom is resolved, the projected band structures of the lower and upper layers clearly reveal that each individual layer retains half-metallic character. The lower and upper layers exhibit opposite spin polarizations: for the lower-layer, spin-up characteristic band crosses the Fermi level, whereas for the upper-layer, spin-down characteristic band inter-

sects the Fermi level. Consequently, AC-stacked bilayer CrS_2 indeed realizes a hidden half-metallic state. Given that the ground state of AA-stacked bilayer CrS_2 is intrinsically antiferromagnetically coupled, a hidden half-metallic state can also be achieved by sliding from the AC to the AA stacking configuration (see FIG.S2[37]). In inversion-asymmetric crystals, the HSP cannot be directly detected unless PT symmetry is broken. Nonetheless, the ARPES and spin-resolved ARPES have already experimentally verified the HSP effect in a variety of materials[11–13]. Hence, the hidden half-metallicity proposed here is also accessible to experimental confirmation by using analogous techniques.

A hidden half-metal can be clearly revealed by applying an out-of-plane electric field to break P symmetry. We apply an electric field of $E=0.05$ V/Å to the AC-stacked bilayer CrS_2 with $d - d_0$ being 0.48 Å. The calculation results show that it still retains an interlayer AFM ground state, which lies 2.5 meV lower in energy than the interlayer-FM state. The total energy band structure along with the spin-resolved projections onto the lower and upper layers are plotted in Figure 4 (a, b, c). It is clearly seen that the spin degeneracy is lifted due to the broken PT symmetry. When the direction of the electric field is reversed, the order of the spin-splitting is

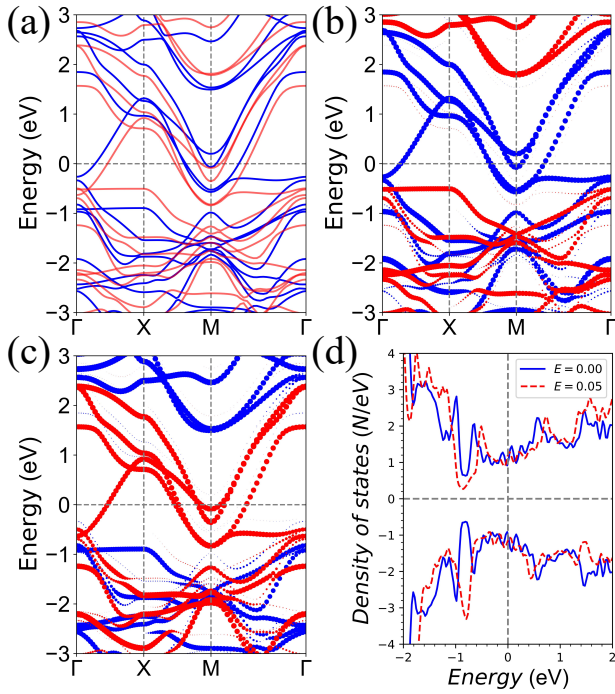


FIG. 4. (Color online) For AC-stacked bilayer CrS_2 with $d - d_0$ being 0.48 \AA , (a, b, c): the total energy band structure along with the spin-resolved projections onto the lower and upper layers at $E=0.05 \text{ V/}\text{\AA}$; (d): the total DOS at $E= 0.00$ and $0.05 \text{ V/}\text{\AA}$. In (a, b, c), the blue, red, and purple curves denote the spin-up, spin-down, and spin-degenerate bands, respectively. In (b, c), the weighting coefficient is proportional to the circle size.

also reversed. Another noteworthy point is that the total magnetic moment is strictly $0.00 \mu_B$, indicating that the AC-stacked bilayer CrS_2 under an applied electric field is a fully-compensated ferrimagnetic metal[40]. According to the projected band structure, the spin-up and spin-down bands near the Fermi level originate predominantly from the lower and upper layers, respectively. By applying an electric field, we can achieve a hidden half-metal in a fully-compensated ferrimagnetic metal. Applying an electric field makes the spin-up and spin-down DOS at the Fermi level differ (see Figure 4 (d)), so the spin-polarized carriers in the lower and upper layers become distinct. This opens a route to electrically manipulate the spin degree of freedom.

Discussion and Conclusion.— The hidden half-metallicity can also be realized in bilayer altermagnets. Here, we illustrate our idea with an unrealistic AB'-stacked bilayer VI_3 as an example (the term "unrealistic" refers to the fact that its ground state is interlayer FM ordering rather than AFM ordering.). Monolayer VI_3 has been shown to be a stable FM half-metal[34], and its crystal structures and energy band structures are presented in FIG.S3[37]. Firstly, the AA'-stacked bilayer is constructed by placing one layer VI_3 on top of another layer VI_3 . The AB'-stacked bilayer is constructed based

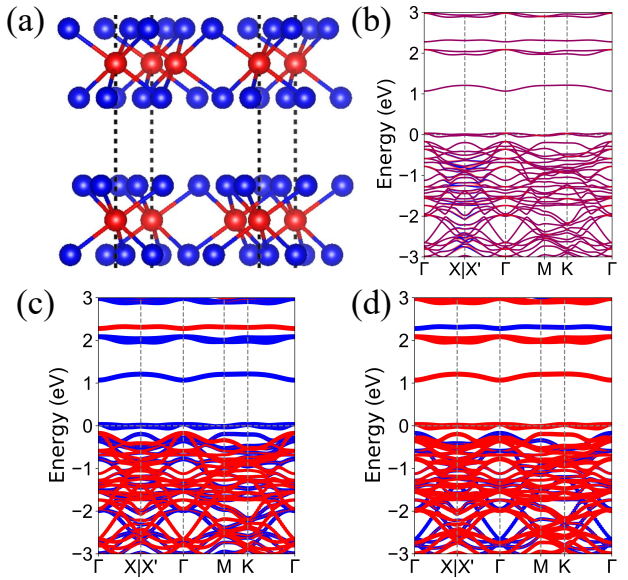


FIG. 5. (Color online) For AB'-stacked bilayer VI_3 , (a): the crystal structures; (b, c, d): the total energy band structure along with the spin-resolved projections onto the lower and upper layers. In (a), the red and blue balls represent V and I atoms, respectively. In (b, c, d), the blue, red, and purple curves denote the spin-up, spin-down, and spin-degenerate bands, respectively. In (c, d), the weighting coefficient is proportional to the circle size.

on the AA' stacking by sliding the top layer horizontally relative to the bottom layer with $2/3\vec{a}+1/3\vec{b}$, which is plotted in Figure 5 (a). For AB'-stacked bilayer VI_3 , the total energy band structure along with the spin-resolved projections onto the lower and upper layers are shown in Figure 5 (b, c, d). To clearly visualize the altermagnetic spin-splitting, an enlarged view of the overall band structure together with the first BZ are plotted in FIG.S4[37]. For AB' stacking, the symmetry operations mainly include C_{3z} , C_{2x} , C_{2y} and C_{2xy} . The C_{3z} symmetry connects atoms within the same spin, while the C_{2x} , C_{2y} and C_{2xy} connect atoms with opposite spins, giving rise to altermagnetic spin-splitting. Although the global band structure shows no half-metallicity, the layer-resolved projected bands unambiguously demonstrate that each individual layer remains half-metallic. Consequently, a hidden half-metal in altermagnets can, in principle, exist.

In summary, we report the concept of a prospective hidden half-metal that exhibits local 100% spin polarization. The system requires spin-antiparallel magnetic atoms to be symmetrically coupled, and is comprised of individual sectors with local half-metallicity. Taking the PT -symmetric bilayer CrS_2 as a representative, we demonstrate that the hidden half-metallicity can be achieved, and an out-of-plane external electric field can be used to tune layer-resolved spin-polarized carriers. Our findings open a new avenue for half-metallic research,

providing both theoretical guidance and material recipes that will enable exploration of its emergent physics.

This work is supported by Natural Science Basis Research Plan in Shaanxi Province of China (2025JC-YBMS-008). We are grateful to Shanxi Supercomputing Center of China, and the calculations were performed on TianHe-2.

* sandongyuwang@163.com

† zhoupan71234@xtu.edu.cn

[1] R. A. de Groot, F. M. Mueller, P. G. van Engen, and K. H. J. Buschow, New class of materials: Half-metallic ferromagnets, *Phys. Rev. Lett.* **50**, 2024 (1983).

[2] B. Dieny, I. L. Prejbeanu, K. Garello, P. Gambardella, P. Freitas, R. Lehnstorff, W. Raberg, U. Ebels, S. O. Demokritov, J. Akerman et al., Opportunities and challenges for spintronics in the microelectronics industry, *Nat. Electron.* **3**, 446 (2020).

[3] L. Šmejkal, J. Sinova and T. Jungwirth, Beyond conventional ferromagnetism and antiferromagnetism: A phase with nonrelativistic spin and crystal rotation symmetry, *Phys. Rev. X* **12**, 031042 (2022).

[4] I. Mazin, Altermagnetism-a new punch line of fundamental magnetism, *Phys. Rev. X* **12**, 040002 (2022).

[5] Y. Liu, S. D. Guo, Y. Li and C. C. Liu, Two-dimensional fully-compensated Ferrimagnetism, *Phys. Rev. Lett.* **134**, 116703 (2025).

[6] S. D. Guo, Valley polarization in two-dimensional zero-net-magnetization magnets, *Appl. Phys. Lett.* **126**, 080502 (2025).

[7] X. Hu, Half-metallic antiferromagnet as a prospective material for spintronics, *Adv. Mater.* **24**, 294 (2012).

[8] S.-J. Gong, C. Gong, Y.-Y. Sun, W.-Y. Tong, C.-G. Duan, J.-H. Chu and X. Zhang, Electrically induced 2D half-metallic antiferromagnets and spin field effect transistors, *Proc. Natl. Acad. Sci. U.S.A.* **115**, 8511 (2018).

[9] Q. Chen, X. Zheng, P. Jiang, Y.-H. Zhou, L. Zhang and Z. Zeng, Electric field induced tunable half-metallicity in an ??-type antiferromagnetic bilayer LaBr₂, *Phys. Rev. B* **106**, 245423 (2022).

[10] X. Zhang, Q. Liu, J. W. Luo, A. J. Freeman and A. Zunger, Hidden spin polarization in inversion-symmetric bulk crystals, *Nat. Phys.* **10**, 387 (2014).

[11] K. Zhang, S. Zhao, Z. Hao, S. Kumar, E. F. Schwier, Y. Zhang, H. Sun, Y. Wang, Y. Hao, X. Ma, C. Liu, L. Wang, X. Wang, K. Miyamoto, T. Okuda, C. Liu, J. Mei, K. Shimada, C. Chen, and Q. Liu, Observation of Spin-Momentum-Layer Locking in a Centrosymmetric Crystal, *Phys. Rev. Lett.* **127**, 126402 (2021).

[12] G. Gatti, D. Gosalbez-Mart ?nez, S. Roth, M. Fanciulli, M. Zucchigna, M. Kallane, K. Rossnagel, C. Jozwiak, A. Bostwick, E. Rotenberg, A. Magrez, H. Berger, I. Vobornik, J. Fujii, O. V. Yazyev, M. Grioni, and A. Crepaldi, Hidden bulk and surface effects in the spin polarization of the nodal-line semimetal ZrSiTe, *Commun. Phys.* **4**, 54 (2021).

[13] W. Yao, E. Wang, H. Huang, K. Deng, M. Yan, K. Zhang, K. Miyamoto, T. Okuda, L. Li, Y. Wang, H. Gao, C. Liu, W. Duan, and S. Zhou, Direct observation of spin-layer locking by local Rashba effect in monolayer semiconducting PtSe₂ film, *Nat. Commun.* **8**, 14216 (2017).

[14] S. Guan, J. X. Xiong, Z. Wang, and J. W. Luo, Progress of hidden spin polarization in inversion-symmetric crystals, *Sci. China-Phys. Mech. Astron.* **65**, 237301 (2022).

[15] J. H. Ryoo and C. H. Park, Hidden orbital polarization in diamond, silicon, germanium, gallium arsenide and layered materials, *NPG Asia Mater.* **9**, e382 (2017).

[16] R. Chen, H. P. Sun, M. Gu, C. B. Hua, Q. Liu1, H. Z. Lu and X. C. Xie, Layer Hall effect induced by hidden Berry curvature in antiferromagnetic insulators, *Natl Sci Rev.* **11**, nwac140 (2024).

[17] S. D. Guo, P. Li and G. Wang, First-principles calculations study of valley polarization in antiferromagnetic bilayer systems, *Phys. Rev. B* **111**, L140404 (2025).

[18] L. D. Yuan, X. Zhang, C. M. Acosta and A. Zunger, Uncovering spin-orbit coupling-independent hidden spin polarization of energy bands in antiferromagnets, *Nat. Commun.* **14**, 5301 (2023).

[19] S. D. Guo, Hidden altermagnetism, *Front. Phys.* **21**, 025201 (2026).

[20] J. Matsuda, H. Watanabe and R. Arita, Multiferroic Collinear Antiferromagnets with Hidden Altermagnetic Spin Splitting, *Phys. Rev. Lett.* **134**, 226703 (2025).

[21] G. Yang, R. Chen, C. Liu et al., Observation of hidden altermagnetism in Cs_{1-δ}V₂Te₂O, arXiv:2512.00972 (2025).

[22] S. D. Guo, Hidden fully-compensated ferrimagnetism, *Phys. Chem. Chem. Phys.* <https://doi.org/10.1039/D5CP03770K>.

[23] Y. Liu, J. Yu and C. C. Liu, Twisted Magnetic Van der Waals Bilayers: An Ideal Platform for Altermagnetism, *Phys. Rev. Lett.* **133**, 206702 (2024).

[24] B. Pan, P. Zhou, P. Lyu, H. Xiao, X. Yang, and L. Sun, General stacking theory for altermagnetism in bilayer systems, *Phys. Rev. Lett.* **133**, 166701 (2024).

[25] S. Zeng and Y.-J. Zhao, Bilayer stacking A-type altermagnet: A general approach to generating two-dimensional altermagnetism, *Phys. Rev. B* **110**, 174410 (2024).

[26] W. Sun, H. Ye, L. Liang, N. Ding, S. Dong and S.-S. Wang, Stacking-dependent ferroicity of a reversed bilayer: Altermagnetism or ferroelectricity, *Phys. Rev. B* **110**, 224418 (2024).

[27] P. Hohenberg and W. Kohn, Inhomogeneous Electron Gas, *Phys. Rev.* **136**, B864 (1964).

[28] W. Kohn and L. J. Sham, Self-Consistent Equations Including Exchange and Correlation Effects, *Phys. Rev.* **140**, A1133 (1965).

[29] G. Kresse, Ab initio molecular dynamics for liquid metals, *J. Non-Cryst. Solids* **193**, 222 (1995).

[30] G. Kresse and J. Furthmüller, Efficiency of ab-initio total energy calculations for metals and semiconductors using a plane-wave basis set, *Comput. Mater. Sci.* **6**, 15 (1996).

[31] G. Kresse and D. Joubert, From ultrasoft pseudopotentials to the projector augmented-wave method, *Phys. Rev. B* **59**, 1758 (1999).

[32] J. P. Perdew, K. Burke and M. Ernzerhof, Generalized gradient approximation made simple, *Phys. Rev. Lett.* **77**, 3865 (1996).

[33] B. Lei, A. Li, W. Zhou, Y. Wang, W. Xiong, Y. Chen and F. Ouyang, Room-temperature ferromagnetism and half-metallicity in monolayer orthorhombic CrS₂. *Front. Phys.* **19**, 43200 (2024).

[34] J. He, S. Ma, P. Lyu and P. Nachtigall, Unusual Dirac half-metallicity with intrinsic ferromagnetism in vanadium trihalide monolayers, *J. Mater. Chem. C* **4**, 2518 (2016).

[35] S. L. Dudarev, G. A. Botton, S. Y. Savrasov, C. J. Humphreys, and A. P. Sutton, Electron-energy-loss spectra and the structural stability of nickel oxide: An LSDA+U study, *Phys. Rev. B* **57**, 1505 (1998).

[36] S. Grimme, S. Ehrlich and L. Goerigk, Effect of the damping function in dispersion corrected density functional theory, *J. Comput. Chem.* **32**, 1456 (2011).

[37] See Supplemental Material at [\[\]](#) for the magnetic configurations; the related stacking structures; the related energy band structures, the related crystal structure and BZ.

[38] R.-Z. Zhang, Y.-Y. Zhang and S. Du, Design of two-dimensional half-metals with large spin gaps, *Phys. Rev. B* **110**, 085130 (2024).

[39] X. Y. Huang, L. M. Zhang, L. Tong, Z. Li, Z. R. Peng, R. F. Lin, W. H. Shi, K. H. Xue, H. W. Dai, H. Cheng, D. D. Branco, J. B. Xu, J. B. Han, G. J. Cheng, X. S. Miao, L. Ye, Manipulating exchange bias in 2D magnetic heterojunction for high-performance robust memory applications, *Nat. Commun.* **14**, 2190 (2023).

[40] S. D. Guo, R. Bian, F.-R. Fan and A. Stroppa, A route to fully-compensated ferrimagnetic metal: electric-field annihilation of the bilayer bandgap, <https://doi.org/10.48550/arXiv.2508.08609> (2025).